

Universal entanglement signatures of quantum liquids as a guide to fermionic criticality

Siddhartha Patra ^{1,*}, Anirban Mukherjee ^{1,†} and Siddhartha Lal ^{1‡}

¹*Department of Physical Sciences, Indian Institute of Science Education and Research-Kolkata, W.B. 741246, India*

(Dated: January 1, 2024)

An outstanding challenge involves understanding the many-particle entanglement of liquid states of quantum matter that arise in systems of interacting electrons. The Fermi liquid (FL) in D spatial dimensions shows a violation of the area-law in real-space entanglement entropy of a subsystem (of length L), $S_{EE} \sim L^{D-1} \ln L$, widely believed to be a hallmark signature of the ground state of a gapless quantum critical system of interacting fermions. In this work, we apply a $T = 0$ renormalisation group approach to a prototype of the FL in momentum (or, k)-space, unveiling thereby the RG relevant long-wavelength quantum fluctuations (due to forward and tangential scattering) from which long-range entanglement arises. A similar analysis of non-Fermi liquids such as the 2D marginal Fermi liquid (MFL) and the 1D Tomonaga-Luttinger liquid (TLL) reveals a universal logarithmic violation of the area-law in gapless electronic liquids for a subsystem defined within a k -space window (of size Λ) proximate to the Fermi surface, with a proportionality constant that depends on the nature of the underlying Fermi surface. We extend this analysis in order to classify the gapped quantum liquids emergent from the destabilisation of the Fermi surface by RG relevant quantum fluctuations arising from backscattering processes. Indeed, we find that the k -space entanglement signatures of gapped quantum liquids appear to be governed by the nature of the Fermi surface (e.g., nested or not) from which they emerge, as well as the nature of their parent gapless metallic liquid (e.g., FL, MFL etc.). The importance of the nature of the Fermi surface is further confirmed by our finding an enhanced entanglement entropy for the nodal MFL present at the quantum critical point recently discovered in the 2D Hubbard model at optimal hole-doping, and lying proximate to a point-like singular Fermi surface. Finally, we report on various quantum information theoretic measures that display the holographic entanglement of various gapless as well as gapped quantum liquids. Our work thus paves the way for an entanglement based classification of various quantum liquids emergent from the criticality of interacting fermionic matter.

INTRODUCTION

There has been a surge recently in applying quantum information-theoretic tools towards understanding the nature of entanglement and quantum correlation encoded within the ground states and low-lying excitations of strongly correlated systems [1–3]. For a system with local interactions among its constituents, the entanglement of a subsystem is expected to follow an area-law (i.e., scale with the size of its boundary) [2]. There are, however, some notable departures. First, a gapped topologically ordered system possesses, in addition to the area-law term, a sub-dominant piece that arises from its topological properties and encodes true long-range entanglement [4–6]. Another exception involves the finding of signatures of volume-law entanglement in some quantum critical systems arising from the existence of gapless quantum fluctuations at all length scales [7–11]. A final exception is found in gapless quantum liquids of interacting electrons in spatial dimensions $d > 1$, and forms the focus of our work. The best understood gapless electronic liquids are metals belonging to the Fermi liquid paradigm [12–14]. These quantum critical systems are known to possess long-range entanglement in the form a modified area-law: $S_{EE} \sim L^{d-1} \ln L$ for d -dimensional subsystem of spatial length L [15–21]. The extra $\ln L$ is conjectured to arise from the presence of gapless long-wavelength quasiparticle excitations lying proximate to a Fermi surface [15, 16, 22–24]. Indeed, this

result is believed to be the higher dimensional analogue of the entanglement scaling observed in quantum critical phases of interacting quantum spin and electron systems in 1D: $S_{EE}^{1D} \sim \ln L$ [25–28]. A similar violation of the area-law is also expected in other quantities of such gapless liquids, such as the fluctuation in the number of particles within a subsystem [29–44].

In addition to the FL, we will also focus here on a particular variant of the 2D non-Fermi liquid known as the marginal Fermi liquid (MFL). Proposed on phenomenological grounds as the parent metal of high-temperature superconductivity in the cuprates [45–47], a first-principles derivation of the effective theory for the MFL (e.g., low-energy Hamiltonian, nature of gapless excitations etc.) was obtained only recently from a detailed renormalisation group study of the 2D Hubbard model [48–50]. Interestingly, the modified area-law discussed above for the real-space entanglement entropy of the FL is also proposed to hold for non-Fermi liquids such as the MFL [51], hinting at a possible universality connecting various gapless electronic quantum liquids despite the obvious differences in some of their key properties (e.g., nature of their low-energy excitations etc.).

Gapless electronic liquids are different. A deeper understanding of the entanglement properties of gapless quantum liquids such as the FL and MFL necessitates an approach that lies beyond the well-established Ginzburg-Landau-Wilson (GLW) paradigm. This can be argued as follows: the effective theories for phases falling within the GLW paradigm describe the quantised excitations of classical scalar (or bosonic) field degrees of freedom that lie above symmetry broken ground states that are short-range entangled at best. On the other hand, the excitations of a

* sp14ip022@iiserkol.ac.in

† am14rs016@iiserkol.ac.in,

‡ slal@iiserkol.ac.in

system of interacting fermions carry sign factors that arise from the exchange of particles and do not have a classical origin. Further, a filled Fermi volume at $T = 0$ is the ground state for gapless fermionic quantum liquids, owes its origin to the Pauli exclusion principle, and is characterised by a topological quantum number called the Luttinger volume that is robust against the inclusion certain kinds of inter-particle interactions [52–58]. Indeed, these liquids are described by effective theories that contain only the physics of the low-energy long-wavelength degrees of freedom proximate to the Fermi surface [59, 60]. The remarkable simplicity of these theories is that they are comprised purely of terms that are number-diagonal in the momentum (or, k)-space single-electron Fock state occupation number operators $\hat{n}_{\vec{k}}$ (see equations eq.(1) and eq.(2) below). This indicates that the k -space many-particle wavefunctions of these quantum liquids are direct product in form, i.e., they are separable in terms of the single-electron Fock states and do not encode any entanglement among them. Instead, as mentioned above, these states of electronic quantum matter display long-range entanglement in real-space. From a renormalisation group (RG) perspective, these low-energy (IR) theories correspond to universal scale-invariant quantum critical fixed points obtained from the coarse-graining of bare (UV) theories of interacting electrons possessing translation invariance.

Setting out the goals. We first seek the quantum fluctuations in the UV from which the real-space long-range entanglement of these universal IR theories is emergent. As the low-energy degrees of freedom in the IR are effectively decoupled from their UV counterparts, meeting this challenge necessitates an investigation of the forward and tangential scattering related RG relevant quantum fluctuations that are resolved under the flow from UV to IR. In keeping with the Wilsonian approach to critical phenomena, this involves understanding the signatures of universality that are likely encoded within the many-particle entanglement wrought from such quantum fluctuations. The answer to this question holds the potential to offer crucial insight on whether certain aspects of the physics of candidate non-Fermi liquids (e.g., the marginal Fermi liquid) show commonalities with metals belonging to the Fermi liquid paradigm, even if some other aspects (e.g., the nature of the low-lying excitations) are qualitatively different. To the best of our knowledge, such a study of the RG evolution of the k -space entanglement has been attempted only for the case of scalar (or bosonic) field theories [61].

Systems of interacting fermions, on the other hand, involve constraints on the inter-particle scattering mechanisms arising from the Pauli exclusion principle as well as phase space constraints due to the existence of a well-defined Fermi volume and a bounding Fermi surface [59, 60]. We recall that the quantum fluctuations in such systems thus contain fermion-exchange related signs, rendering their study difficult. Recent studies indicate that the sign structure of the many-particle wavefunction significantly affects the nature of the entanglement encoded in them [62, 63]. This is of particular significance to the study of non-Fermi liquid gapless states that are emergent at quantum critical points related to the collapse of a Fermi liquid metal: a recent numerical study based on an ansatz wavefunction

incorporating correlations from long-ranged backflow effects of the interacting fermions revealed a crossover from a volume-law scaling of the subsystem entanglement entropy to the modified area-law familiar for the Fermi liquid effective theory [64]. The crossover takes place across a distance scale related to the physics of critical backflow interactions. In addition, it is pertinent to enquire on whether there exist similar imprints of universality hidden within the backscattering related RG relevant quantum fluctuations that destabilise the Fermi surface of these gapless metallic states and lead to the emergence of topologically ordered gapped liquid states of quantum matter (e.g., the 2D Mott liquid found in the 2D Hubbard model on the square lattice at 1/2-filling [48] and the Cooper pair insulator for the reduced BCS model with a circular Fermi surface [65]). This amounts to an attempt at a systematic classification of the states of quantum matter based on their entanglement content, and looks beyond the short range entangled states that belong to the Ginzburg-Landau-Wilson paradigm of broken symmetries and real-space local order parameters.

The strategy. In order to meet these goals, we adopt a RG approach that we have formulated recently for the investigation of criticality observed in systems of interacting fermions [48–50, 57, 58, 65, 66]. Formulated using only many-particle unitary transformations to the bare Hamiltonian, the procedure reveals IR fixed point theories and their low-energy wavefunctions. An iterative application of the unitaries to the IR wavefunctions then generates a family of states spanning towards the UV. This facilitates a quantitative study of the RG evolution of many-body correlations, as well as several many-particle entanglement features, from the ground state and lowest lying excited states [58, 65, 67, 68]. Thus, we first employ this strategy to obtain the UV wavefunctions of several gapless and gapped quantum liquid states that are unitarily connected to their IR counterparts. We then compute the scaling of the entanglement entropy of a block of states in k -space (lying proximate to the IR Fermi energy) with the block size (Λ).

RESULTS

Models of gapless liquids. The IR fixed point Hamiltonian describing the excitations of the FL phase is [12–14]

$$H_{FL}^{\hat{s}} = \sum_{k,\sigma} \epsilon_k n_{k\sigma} + \sum_{\substack{kk' \in \{\hat{s}, \hat{s}'\} \\ \sigma, \sigma'}} V_{kk'\sigma\sigma'} n_{k,\sigma} n_{k',\sigma'}, \quad (1)$$

where \hat{s} and \hat{s}' correspond to excitations in directions normal to the Fermi surface, and an analytic expression for the RG evolution of the interaction coupling $V_{kk'\sigma\sigma'}$ has been obtained from a unitary renormalisation group (URG) study of the 2D Hubbard model on the square lattice at large hole doping (see Methods and Supplementary Materials Note I) [49, 50]. Further, the IR fixed point effective Hamiltonian for the MFL phase is obtained from the URG analysis of the 2D Hubbard model at half-filling, as well as

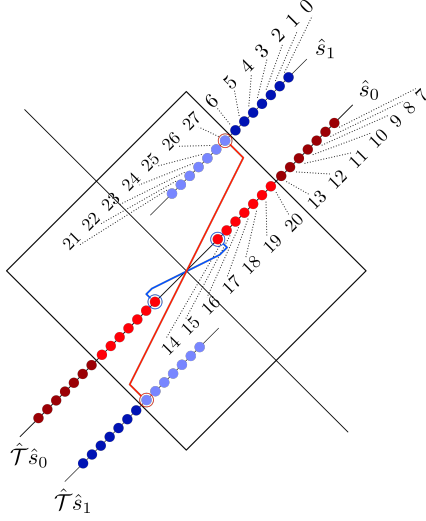


FIG. 1. **Momentum-space construction of prototypical system studied under MERG.** Four directions ($\hat{s}_0, \hat{s}_1, \hat{T}\hat{s}_0, \hat{T}\hat{s}_1$) are chosen normal to the Fermi surface in the 2D Brillouin zone; two ($\hat{s}_0, \hat{T}\hat{s}_0$, lines of red circles) are labelled as the nodal directions, and two ($\hat{s}_1, \hat{T}\hat{s}_1$, lines of blue circles) as the near-anti-nodal. Each \hat{s} -direction is comprised of 28 electronic Fock states (red and blue circles). A reduced subspace corresponds to pseudospins formed from electrons with opposite momenta (\vec{k} and $-\vec{k}$) (bold red and blue lines).

optimal doping, as as [48–50]

$$H_{MFL}^{\hat{s}} = \sum_{k,\sigma} \epsilon_k n_{k\sigma} + \sum_{\substack{\vec{K}=(k k' k'' \sigma) \\ k k' k'' \in \hat{s} \\ \sigma}} \mathcal{R}_{\vec{K}}^{\hat{s}} n_{k,\sigma} n_{k',-\sigma} \left(1 - n_{k'',\sigma}\right) \quad (2)$$

where the RG evolution for the interaction coupling $\mathcal{R}_{\vec{K}}^{\hat{s}}$ is shown in the Supplementary Materials Note I. We can see from eq.(2) that the low-lying excitations of the MFL are described by three-particle composite objects comprised of two electrons and a hole. Further, various features conjectured for the MFL phenomenology (e.g., the vanishing of the Landau quasiparticle residue at energies proximate to the Fermi surface [45–47]) have been established from the MFL effective Hamiltonian eq.(2) [48–50]. Importantly, all backscattering related quantum fluctuations in k -space are rendered irrelevant under the RG flows to the FL and MFL fixed point theories. On the other hand, quantum fluctuations arising from RG relevant forward and tangential scattering processes of interacting electrons are of interest in understanding the nature of the entanglement. Finally, in unveiling the entanglement features of the gapped quantum liquids (e.g., Mott liquid, Cooper pair insulator) obtained by destabilising the FL and MFL fixed points, we will consider the quantum fluctuations arising from RG relevant backscattering processes.

Forming a prototypical system. Our investigations of entanglement involve simulating the RG evolution of many-body wavefunctions. For this, we apply iteratively the inverse many-particle unitary transformations of the URG method to the IR ground state wavefunction of, say, the FL (see Method). This generates quantum fluctuations by coupling the electronic Fock states near the Fermi surface

to those farther away via forward and tangential scattering processes. In this way, we obtain a family of wavefunctions ranging from IR to UV, and involving a systematic growth of the size of the effective Hilbert space of interacting electrons. This k -space entanglement renormalisation group (MERG) process is, however, rendered very challenging due to the fact that the many-particle Hilbert space scales exponentially in the system size. In order to make the MERG analysis tractable, we construct a smaller prototype of the FL and MFL systems in k -space for an underlying 2D square lattice (Fig.1). We begin by dividing the window of low-momenta around the Fermi surface into several directions normal to it, and consider only the quantum fluctuations generated by scattering processes along only four such directions ($\hat{s}_0, \hat{s}_1, \hat{T}\hat{s}_0, \hat{T}\hat{s}_1$). The direction \hat{s}_0 and its inverse ($\hat{T}\hat{s}_0$) are along the nodal direction of the square Brillouin zone, while \hat{s}_1 and its inversion ($\hat{T}\hat{s}_1$) are near the antinodal direction.

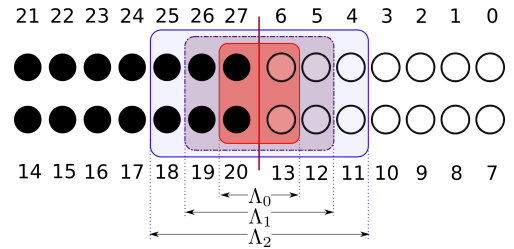


FIG. 2. **Progression of the MERG flow.** The black circles represent up-pseudospins (pairs of occupied electronic Fock states), and the white circles represent down-pseudospins (pairs of unoccupied electronic Fock states). The red vertical line represents the Fermi surface. The red shaded box represents the k -space window (Λ_0) of the IR fixed point theory, while the light purple and light blue shaded boxes represent the windows (Λ_1 and Λ_2) of electronic Fock states coupled by quantum fluctuations after the first and second steps of the MERG respectively.

As a study of the 112 fermionic states in the prototype (i.e., a Hilbert space dimension of $\sim 10^{33}$) is intractable, we focus the study on the quantum fluctuations of the holon (pairs of unoccupied electronic Fock states) and doublon (pairs of occupied electronic Fock states) degrees of freedom in the hole-doped 2D Hubbard model. As shown in Fig.1, this corresponds to a smaller sub-space defined in terms 56 pseudospin degrees of freedom (defined in terms of electronic Fock states with opposite momenta) and a reduced Hilbert space size $\sim 10^{16}$ [48, 49, 68, 69]. A further drastic simplification is made by ignoring the RG irrelevant backscattering related quantum fluctuations: this allows us to study the problem of 28 pseudospins residing on only one side of the Brillouin zone, say, the \hat{s}_0 and \hat{s}_1 directions. In each of these directions, we have chosen 14 pseudospin states, seven outside and seven inside the Fermi surface. As shown in Fig.2, the MERG proceeds via the iterative application of a set of unitaries ($U_{(j)}^\dagger$, $j \in \{1, 2, \dots, 6\}$) to the IR fixed point ground state and lowest-lying excited state wavefunctions of the gapless FL and MFL liquids that systematically couple the 4 electronic Fock states (6, 13, 20, 27) lying within the window proximate to the Fermi surface to the 24 Fock states lying outside. The detailed form of $U_{(j)}$ is given in the Methods and Supplementary Materials Note

I.

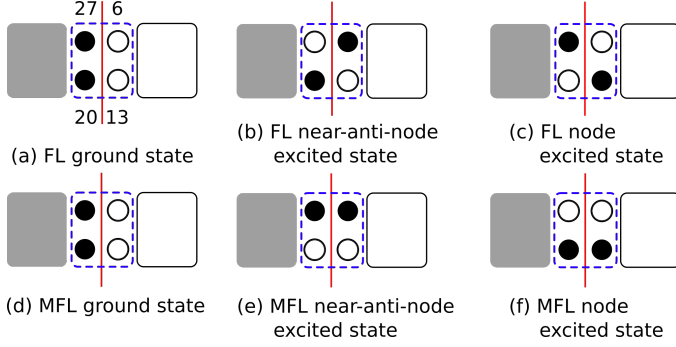


FIG. 3. **Construction of ground and lowest-lying excited states of FL and MFL.** The black circles represent up-pseudospins (pairs of occupied electronic Fock states), and the white circles represent down-pseudospins (pairs of unoccupied electronic Fock states). The red color vertical line in the middle represents the Fermi surface, while the grey and white boxes represent the occupied and unoccupied states below and above the Fermi surface respectively. The blue dashed box represents the window of the IR gapless quantum liquid. (a) FL ground state configuration: all states occupied inside the Fermi surface, and unoccupied outside. (b) FL excited state, with excitation in the near-anti-nodal direction. (c) FL excited state, with excitation in the nodal direction. (d) MFL ground state configuration (identical to that of the FL). (e) MFL excited state, with excitation in the near-anti-nodal direction. (f) MFL excited state, with excitation in the nodal direction.

The IR wavefunctions for the ground state and lowest-lying excited states of the prototypical system taken for the FL and MFL phases in shown in Fig.3. The IR fixed-point ground state involving the four Fock states (6, 13, 20, 27) are identical for both the FL and MFL (see Fig.3(a, d)): all state below the Fermi surface are occupied, and those above it are unoccupied. This is a consequence of the fact that both these gapless liquids have been established as satisfying Luttinger's theorem [52–58]. The lowest lying excited states of the FL and MFL involve configurations with holes below the Fermi surface and occupied states above it. We consider two such possible excited states in the prototypical model: the near-anti-node (Fig.3(b) for the FL and (e) for the MFL) and nodal (Fig.3(c) for the FL and (f) for the MFL) excited states. The IR ground state of the FL is written in terms of the pseudospin degrees of freedom as $|\Psi_0^{FL}\rangle = |\phi_E^{FL}\rangle \otimes |\Psi_{IOM}\rangle_{(0)}$, where $|\phi_E^{FL}\rangle = |\uparrow_{20}\uparrow_{27}\rangle \otimes |\downarrow_6\downarrow_{13}\rangle$ represents the window of Fock states (6, 13, 20, 27) proximate to the Fermi surface and the configuration of the Fock states lying outside these windows (whose occupation numbers correspond to integrals of motion (IOMs) of the URG method) is given by

$$|\Psi_{IOM}\rangle_{(0)} = \prod_{i=0}^5 |\downarrow_i\rangle \otimes \prod_{i=7}^{12} |\downarrow_i\rangle \otimes \prod_{i=14}^{19} |\uparrow_i\rangle \otimes \prod_{i=21}^{26} |\uparrow_i\rangle \quad (3)$$

The first step of the MERG then couples the four Fock states (5, 12, 19, 26) with (6, 13, 20, 27) via the application of the unitary operator $\mathcal{U}_{(6)}^\dagger: |\Psi_1^{FL}\rangle = \mathcal{U}_{(6)}^\dagger |\Psi_0^{FL}\rangle$, and so onwards till we obtain a UV wavefunction that is unitarily connected to the IR state we started from.

We then employ the UV wavefunction to study the scaling of the von-Neumann entanglement entropy of a subsystem in k -space with its size. This is done by first selecting a block in k -space of size (2Λ) , chosen symmetrically about the Fermi surface and along the \hat{s}_0 and \hat{s}_1 directions. Small k -space blocks contain degrees of freedom corresponding to the largest real-space lengthscales and vice versa. By tracing over all degrees of freedom except those within the chosen block, a reduced density matrix is then obtained for the block (ρ_Λ). The von-Neumann entanglement entropy ($S_{EE} = -\text{Tr}[\rho_\Lambda \ln \rho_\Lambda]$) is computed for the k -space block. Understanding the entanglement signatures in the UV wavefunctions of FL and MFL ($|\Psi_j\rangle$, $j > 0$) is the primary goal of this work.

Scaling of S_{EE} for gapless quantum liquids : Fig.4(a) and Fig.4(c) show the scaling of S_{EE} k -space block size (Λ) along the nodal direction of the UV ground states of the FL and MFL obtained from the optimally doped and overdoped 2D Hubbard model respectively. Both gapless quantum liquids show logarithmic scaling of block entanglement in k -space with decrease in block size Λ , i.e., upon focusing on quantum fluctuations lying proximate to the Fermi surface: $S_{EE} \sim \ln \Lambda$. Further, the number fluctuations ($\Delta N = \sqrt{\langle N^2 \rangle - \langle N \rangle^2}$) within the block Λ also show similar logarithmic scaling for both the FL and MFL: $\Delta N \sim \ln \Lambda$, as shown in Fig.4(b) and Fig.4(d) respectively. These results correspond to a modified area-law for these gapless liquids (upon accounting for all directions normal to the Fermi surface): $S_{EE}^{\text{gapless}} \sim \Lambda \ln \Lambda$. Further, this confirms the existence of long-range entanglement in k -space encoded within the UV wavefunctions of both these gapless quantum liquids, arising from long-wavelength quantum fluctuations at low energies.

The results for the scaling of S_{EE} with Λ for the two excited state configurations (i.e., along the nodal (\hat{s}_0) and near-anti-nodal (\hat{s}_1) directions normal to the Fermi surface) of the FL and MFL phases are shown in Figs.4(e), 4(f) and Figs.4(g), 4(h) respectively. While all results show a logarithmic scaling for S_{EE} with Λ , $S_{EE} \sim (1/\alpha) \ln \Lambda$, the values of the coefficient α_{FL} are similar for the two excited states of the FL ($\alpha_{FL} \sim 2$). This likely arises from the presence of strong forward scattering normal to the Fermi surface, as well as tangential scattering between the two \hat{s} directions. On the other hand, the values of α_{MFL} are quite different for the two excited states of the MFL, and $\alpha_{MFL} \gg \alpha_{FL}$. This displays the strong electronic differentiation among the \hat{s} directions in the MFL phase, and the fact that only strong forward scattering processes determine the entanglement of this gapless liquid. Further, we have also found that both the 2D Fermi liquid with circular Fermi surface and the 1D Tomonaga-Luttinger liquid show logarithmic scaling behaviour of S_{EE} with Λ . In Fig.5(a) and (b), we show that the coefficient $\alpha \rightarrow 2$ for both these gapless quantum liquids upon computing the S_{EE} from wavefunctions after a sufficiently large number of MERG steps. These results suggest that while the Fermi liquid and several non-Fermi liquids show the same modified area-law for the scaling of S_{EE} with Λ , the value of the proportionality constant $1/\alpha$ is sensitive to the nature of the underlying Fermi surface.

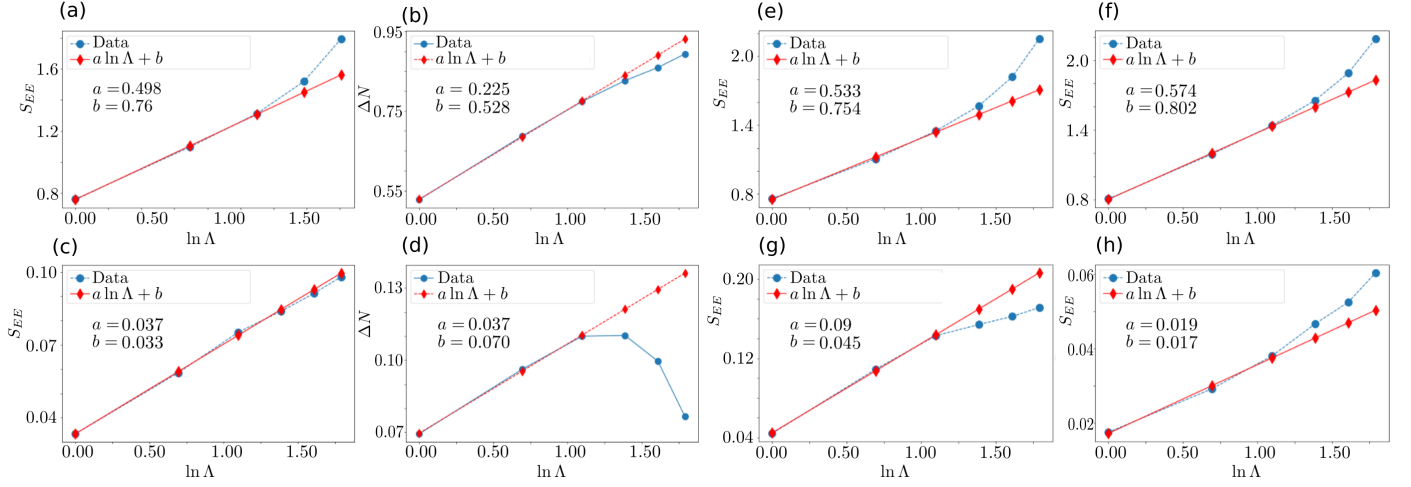


FIG. 4. **Scaling of entanglement entropy (S_{EE}) and number fluctuations (ΔN) within a window in k -space with window size (Λ) for gapless liquids.** (a) S_{EE} and (b) ΔN for FL ground state along the nodal direction \hat{s}_0 . (c) S_{EE} and (d) ΔN for MFL ground state along the nodal direction \hat{s}_0 . (e) and (f) show scaling of S_{EE} for excited states of FL along nodal (\hat{s}_0) and antinodal (\hat{s}_1) directions respectively. Similarly, (g) and (h) show scaling of S_{EE} for excited states of MFL along nodal (\hat{s}_0) and antinodal (\hat{s}_1) directions respectively.

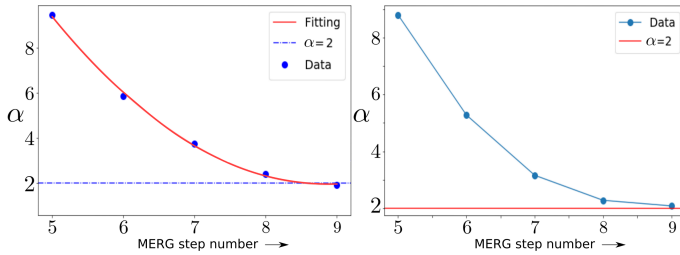


FIG. 5. **Variation of the inverse slope (α) of the scaling of S_{EE} with $\ln \Lambda$ with number of MERG steps.** The coefficient α is observed to saturate to $\alpha \sim 2$ for (a) the Fermi liquid in two dimensions with a circular Fermi surface, and (b) the Tomonaga-Luttinger liquid in one dimension.

Scaling of S_{EE} for gapped quantum liquids : In order to understand whether k -space entanglement is a good diagnostic of fermionic criticality, we need to study RG relevant quantum fluctuations of various kinds. Having accounted above for the forward and tangential scattering related quantum fluctuations that lead to gapless quantum liquids, we now turn to the gapped quantum liquids that arise from backscattering. The ground state wavefunctions for the states studied below have been obtained from Refs.[48, 49, 58, 65], and adopted to the prototypical system shown in Figs.1 and 2 similarly to that discussed earlier for gapless liquids. Fig.6(a) shows the linear scaling of S_{EE} with Λ for the gapped 2D Mott liquid along the nodal direction \hat{s}_0 , and reflects a volume-law scaling upon accounting for all directions normal to the Fermi surface: $S_{EE}^{gapped} \sim \Lambda^2$. This enhancement in S_{EE} (with regards to that observed for the gapless liquids) arises from quantum fluctuations associated with RG relevant backscattering processes in the 1/2-filled 2D Hubbard model (due to a strongly nested Fermi surface of the underlying 2D tight-binding model) [48]. On the other hand,

in Fig.6(b), we see that the scaling of S_{EE} with Λ for a gapped 2D Cooper pair insulator phase along a given direction normal to a circular (i.e., non-nested) Fermi surface shows the modified area-law observed for the gapless 2D FL: $S_{EE} \sim (1/\alpha) \ln \Lambda$ with a coefficient $\alpha \sim 2$. Further, the nature of the parent metal (from which these gapped phases are emergent) also appears to be an important factor: the MFL is the parent metal for the 2D Mott liquid [48, 50], while the FL is the parent metal for the CPI studied in Fig.6(b) [65].

In order to understand the dependence of these scaling laws of S_{EE} on the nature of the underlying Fermi surface, we studied the case of the quantum critical point obtained recently in the optimally-doped 2D Hubbard model [49]: here, the four nodal directions contain gapless MFL liquids while the rest of the Fermi surface is composed of a gapped 2D Cooper pair insulator liquid. Thus, in Figs.6(c) and (d), we present the scaling of S_{EE} with Λ for the nodal MFL (along \hat{s}_0) and near-anti-nodal CPI liquid (along \hat{s}_1) respectively. While the CPI again shows the logarithmic scaling behaviour (albeit with a coefficient $\alpha < 1$), the MFL shows linear scaling of S_{EE} with Λ and reflects on an enhanced long-range entanglement along the nodal directions due to an underlying quantum critical Fermi surface.

DISCUSSIONS

A modified area-law in k -space. By studying a prototype of the k -space scattering processes (i.e., along and between certain directions normal to the Fermi surface), our results reveal a modified area-law scaling in both the block entanglement (S_{EE}) and number fluctuations (ΔN) for the UV ground states and lowest lying excited states unitarily connected to the Fermi liquid (FL), marginal Fermi liquid (MFL) and Tomonaga-Luttinger liquid (TLL) gapless quantum liquids (Figs.4 and 5) : $S_{EE} \propto \log(\Lambda/\Lambda_F)$ and

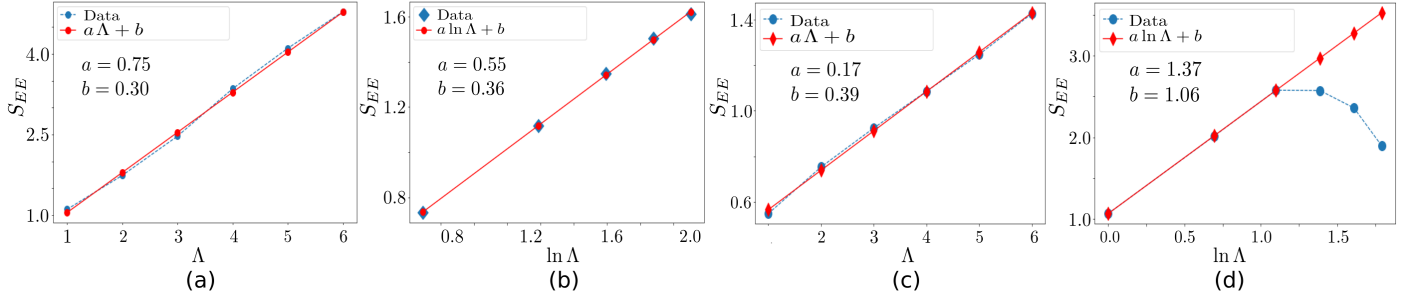


FIG. 6. **Scaling of entanglement entropy (S_{EE}) with window size (Λ) for gapped liquids.** (a) 2D Mott liquid along nodal (\hat{s}_0) direction of a 2D nested Fermi surface. (b) 2D Cooper pair insulator (CPI) along a radius of the circular Fermi surface. (c) and (d): Scaling of S_{EE} with Λ for gapless MFL along nodal direction (\hat{s}_0) and 2D CPI along near-anti-nodal direction (\hat{s}_1) at the quantum critical point of the optimally hole-doped 2D Hubbard model [49] respectively.

$\Delta N \propto \log(\Lambda/\Lambda_F)$ (where Λ_F is the Fermi momentum, and which we set to unity hereafter). This is in agreement with findings for the real-space block entanglement entropy and number fluctuations computed from the IR state of the FL, and reveals that the forward and tangential scattering related RG relevant quantum fluctuations near the Fermi surface encode the long-range k -space entanglement of the modified area-law even at UV scales. This is consistent with the conjectured duality mapping between the real-space and k -space subsystem entanglement entropies of a system of non-interacting fermions in d -spatial dimensions [70]. Further, it shows that the k -space quantum fluctuations of the UV theory are systematically converted into their real-space counterparts along the URG flow.

Universality of Gapless Liquids. Importantly, the similarity of the results obtained for both FL, MFL and TLL offer striking evidence on the universality of the entanglement properties of various gapless quantum liquids that arise from systems of interacting electrons. This suggests a unification of the Fermi liquid paradigm with non-Fermi liquid metals that are qualitatively different in terms of their low-lying excitations. Interestingly, we find that the proportionality constant α in the relation $S_{EE} \propto (1/\alpha) \ln \Lambda$ is very different for the different metallic systems: $\alpha \sim 2$ for the FL (whether obtained from a 2D Fermi volume with a $U(1)$ symmetric circular Fermi surface (Fig.5(a)), or from the strongly rounded $C(4)$ symmetric Fermi surface of the FL obtained in the 2D Hubbard at large hole-doping [49] (Fig.4(a), (b), (e) and (f))) and the TLL (with a 2 point Fermi surface, Fig.5(b)). On the other hand, we find $\alpha \gg 1$ for the MFL obtained in the 2D Hubbard at optimal hole-doping [49] (Fig.4(c), (d), (g) and (h))). We believe that this difference arises from the fact that the MFL is governed by strongly RG relevant forward scattering in directions normal to the Fermi surface, and that MFL states on different normals show variations arising from the differentiation in the electronic dispersion everywhere along the $C(4)$ symmetric Fermi surface of the 2D square lattice [48, 49]. By contrast, the presence of subdominant RG relevant tangential scattering processes in the FL between different directions normal to the Fermi surface remove the electronic differentiation inherent in the MFL [49].

Classification of Gapped Quantum Liquids. We also analyse the k -space block entanglement entropy (S_{EE}) of the UV states that are unitarily connected to the gapped

topologically ordered quantum liquids emergent from the destabilisation of the Fermi surface of the FL and MFL gapless metals [48–50, 65]. As shown in Figs.6(a) and (b), we find that while the Cooper pair insulating (CPI) state for the 2D FL with circular Fermi surface [65] shows logarithmic scaling of S_{EE} with Λ (with the inverse coefficient $\alpha \sim 2$), the Mott liquid state in the 2D Hubbard model at 1/2-filling [48, 50] shows a volume-law scaling with Λ . We believe that this striking difference arises from the fact that the 2D Mott liquid is emergent from the backscattering related instability of a strongly nested singular Fermi surface of the underlying 2D tight-binding model (i.e., containing van Hove singularities), while the 2D CPI state emergent from the minimal nesting of a circular Fermi surface (i.e., that of diametrically opposite Fermi points). Further, the parent metal of the former is the 2D MFL [48], while that of the latter is the 2D FL [65]. Thus, we conclude that the entanglement features of a gapped quantum liquid appear to be determined by the nature of the Fermi surface and parent metal from which it emerges. Further evidence of this dependence is seen by considering the scaling behaviour of the k -space block entanglement entropy (S_{EE}) of the quantum critical state of matter found recently in the 2D Hubbard model on the square lattice at optimal doping [49]. At this novel quantum critical point (QCP), only the four nodal directions of the 2D Brillouin zone for the square lattice are found to be comprised of gapless metallic MFLs, while there exists a gapped 2D CPI quantum liquid in the antinodal regions of the rounded $C(4)$ symmetric hole-doped Fermi surface of the underlying 2D tight-binding model. We find that S_{EE} scales logarithmically with Λ for this 2D CPI state (Fig.6(d)), while the nodal MFLs (about four point-like singular quantum critical Fermi surfaces) show a volume-law scaling (Fig.6(c)). Indeed, this appears to be consistent with the findings of Ref.[64] for S_{EE} of a gapless metal at a quantum critical Fermi surface.

Holographic evolution of entanglement. Finally, the unitary renormalisation group (URG) method has also been shown to provide an explicit demonstration of the holographic principle [71, 72]. By this, we mean that the evolution of the Hamiltonian from UV to IR via the unitaries corresponds to a tensor network that admits an exact holographic mapping, i.e., it provides a precise relationship between the coupled degrees of freedom within one

layer of the network with those that are emergent in the next [73, 74]. Further, this generates a eigenstate coefficient tensor network possessing an entanglement metric [57]. The renormalisation of the entanglement corresponds to the evolution of the many-particle Hilbert space geometry. By employing this method, we unveil the distinct holographic signatures of Fermi and non-Fermi liquids, as well as the gapped states reached by their destabilisation (see Supplementary Materials Notes II and III). An important challenge for the future will be to characterise the entanglement properties of gapless liquids using multipartite quantum information measures, as has been achieved recently for topologically ordered gapped liquids [75].

METHOD

Momentum-space Entanglement RG. The MERG method involves the iterative application of a set of many-particle unitary transformations applied to, say, the ground state wavefunction ($|\Psi_0\rangle$) of an IR effective theory (and characterised by a quantum fluctuation energyscale ω)

$$\mathcal{U}_{j+1}^\dagger |\Psi_{(j)}(\omega)\rangle = |\Psi_{(j+1)}(\omega)\rangle, \quad 0 \leq j < N. \quad (4)$$

This generates a series of wavefunctions ($|\Psi_{(j)}\rangle, 0 \leq j < N$) that connect unitarily between the IR state ($j = 0$) and the state in the UV ($j = N$). The unitaries (\mathcal{U}_j^\dagger) are obtained from the $T = 0$ unitary renormalisation group (URG) used to derive the low energy effective Hamiltonian for various strongly correlated gapless and gapped phases of matter [48–50, 57, 58, 65, 66]. The URG iteratively decouples quantum fluctuations in the higher energy Fock states of a bare (or UV) Hamiltonian by applying many-body unitary operators ($U_{(j)}$), generating a flow towards a low-energy effective Hamiltonian in the IR. For a bare Hamiltonian of interacting electrons ($\mathcal{H}_{(N)}$) possessing a total number of N Fock states, we begin by labelling the Fock states according to their energies ($\epsilon_N > \epsilon_{N-1} > \dots$) of the diagonal part of the Hamiltonian (H^D). Mutually non-commuting terms in the Hamiltonian are the source of quantum fluctuations in the Fock states and characterised by an energyscale ω . Thus, the application of the unitary operator \mathcal{U}_N then removes quantum fluctuations present in

the N^{th} Fock state, and leads to a new Hamiltonian

$$\mathcal{H}_{(N-1)} = \mathcal{U}_N \mathcal{H}_{(N)} \mathcal{U}_N^\dagger. \quad (5)$$

\mathcal{U}_{N-1} is then applied in order to remove the quantum fluctuations in the Fock state $N - 1$, and so on. The general form of the unitary operator ($U_{(j)}$) for the j^{th} step of URG is give as

$$\begin{aligned} \mathcal{U}_j &= (1 + \eta_j - \eta_j^\dagger)/\sqrt{2}, \\ \eta_j^\dagger &= \frac{1}{\omega - \text{Tr}(\mathcal{H}_{(j)} \hat{n}_j)} c_j^\dagger \text{Tr}(\mathcal{H}_{(j)} c_j). \end{aligned} \quad (6)$$

An equivalence of the quantum fluctuation scale ω with an energyscale for finite-temperature thermal fluctuations has also been established in Refs.[48–50, 57]. The IR fixed point effective theory ($\mathcal{H}_{(j^*)}$) is reached when further decoupling is not possible (as the denominator of η_{j^*} vanishes) [57]. The URG has been applied in deriving analytic expressions for the low-energy effective theories of several gapless as well as gapped quantum liquid states of matter discussed in the main text (e.g., FL, MFL, Mott liquid, CPI, TLL, etc.) [48–50, 57, 58, 65, 66]. Upon deriving the low-energy effective fixed point Hamiltonian ($\mathcal{H}_{(j^*)}(\omega)$) we solve for the ground state and low-lying excited states ($|\Psi_{(j^*)}(\omega)\rangle$). The MERG involves a numerical simulation of the inverted RG flow (i.e., from IR to UV) for these wavefunctions, and enables the computation of various entanglement features encoded within them.

ACKNOWLEDGMENTS

The authors thank S. Pal, Abhirup Mukherjee, R. K. Singh, A. Dasgupta, A. Ghosh, S. Sinha and A. Taraphder for several discussions and feedback. S. P. and A. M. thanks the CSIR, Govt. of India and IISER Kolkata for funding through research fellowships. S. Lal thanks the SERB, Govt. of India for funding through MATRICS grant MTR/2021/000141 and Core Research Grant CRG/2021/000852.

-
- [1] B. Zeng, X. Chen, D.-L. Zhou, X.-G. Wen, *et al.*, *Quantum information meets quantum matter* (Springer, 2019).
 - [2] J. Eisert, M. Cramer, and M. B. Plenio, Colloquium: Area laws for the entanglement entropy, *Reviews of modern physics* **82**, 277 (2010).
 - [3] N. Laflorencie, Quantum entanglement in condensed matter systems, *Physics Reports* **646**, 1 (2016), quantum entanglement in condensed matter systems.
 - [4] M. A. Levin and X.-G. Wen, String-net condensation: A physical mechanism for topological phases, *Phys. Rev. B* **71**, 045110 (2005).
 - [5] A. Kitaev and J. Preskill, Topological entanglement entropy, *Phys. Rev. Lett.* **96**, 110404 (2006).
 - [6] A. Hamma, R. Ionicioiu, and P. Zanardi, Bipartite entanglement and entropic boundary law in lattice spin systems,

- Phys. Rev. A* **71**, 022315 (2005).
- [7] E. S. Sørensen, M.-S. Chang, N. Laflorencie, and I. Affleck, Quantum impurity entanglement, *Journal of Statistical Mechanics: Theory and Experiment* **2007**, P08003 (2007).
- [8] V. Alba, M. Fagotti, and P. Calabrese, Entanglement entropy of excited states, *Journal of Statistical Mechanics: Theory and Experiment* **2009**, P10020 (2009).
- [9] B. Pozsgay, Algebraic construction of current operators in integrable spin chains, *Physical Review Letters* **125**, 070602 (2020).
- [10] L. Wang, D. Poilblanc, Z.-C. Gu, X.-G. Wen, and F. Verstraete, Constructing a gapless spin-liquid state for the spin-1/2 j 1- j 2 heisenberg model on a square lattice, *Physical review letters* **111**, 037202 (2013).

- [11] C. Peng, Y.-F. Jiang, Y. Wang, and H.-C. Jiang, Gapless spin liquid and pair density wave of the hubbard model on three-leg triangular cylinders, *New Journal of Physics* **23**, 123004 (2021).
- [12] L. Landau, The theory of a fermi liquid, *JETP* **3**, 920 (1956).
- [13] L. Landau, Oscillations in a fermi liquid, *JETP* **5**, 101 (1957).
- [14] L. Landau, On the theory of the fermi liquid, *JETP* **8**, 70 (1959).
- [15] B. Swingle, Entanglement entropy and the fermi surface, *Phys. Rev. Lett.* **105**, 050502 (2010).
- [16] B. Swingle, Conformal field theory approach to fermi liquids and other highly entangled states, *Phys. Rev. B* **86**, 035116 (2012).
- [17] M. M. Wolf, Violation of the entropic area law for fermions, *Phys. Rev. Lett.* **96**, 010404 (2006).
- [18] D. Gioev and I. Klich, Entanglement entropy of fermions in any dimension and the widom conjecture, *Phys. Rev. Lett.* **96**, 100503 (2006).
- [19] W. Li, L. Ding, R. Yu, T. Roscilde, and S. Haas, Scaling behavior of entanglement in two- and three-dimensional free-fermion systems, *Phys. Rev. B* **74**, 073103 (2006).
- [20] T. Barthel, M.-C. Chung, and U. Schollwöck, Entanglement scaling in critical two-dimensional fermionic and bosonic systems, *Phys. Rev. A* **74**, 022329 (2006).
- [21] S. Farkas and Z. Zimborás, The von neumann entropy asymptotics in multidimensional fermionic systems, *Journal of Mathematical Physics* **48**, 102110 (2007).
- [22] R. Helling, H. Leschke, and W. Spitzer, A Special Case of a Conjecture by Widom with Implications to Fermionic Entanglement Entropy, *International Mathematics Research Notices* **2011**, 1451 (2010).
- [23] H. Leschke, A. V. Sobolev, and W. Spitzer, Scaling of rényi entanglement entropies of the free fermi-gas ground state: A rigorous proof, *Phys. Rev. Lett.* **112**, 160403 (2014).
- [24] W. Ding, A. Seidel, and K. Yang, Entanglement entropy of fermi liquids via multidimensional bosonization, *Phys. Rev. X* **2**, 011012 (2012).
- [25] A. Osterloh, L. Amico, G. Falci, and R. Fazio, Scaling of entanglement close to a quantum phase transition, *Nature* **416**, 608 (2002).
- [26] T. J. Osborne and M. A. Nielsen, Entanglement in a simple quantum phase transition, *Phys. Rev. A* **66**, 032110 (2002).
- [27] G. Vidal, J. I. Latorre, E. Rico, and A. Kitaev, Entanglement in quantum critical phenomena, *Phys. Rev. Lett.* **90**, 227902 (2003).
- [28] P. Calabrese and J. Cardy, Entanglement entropy and quantum field theory, *Journal of Statistical Mechanics: Theory and Experiment* **2004**, P06002 (2004).
- [29] I. Klich, G. Refael, and A. Silva, Measuring entanglement entropies in many-body systems, *Phys. Rev. A* **74**, 032306 (2006).
- [30] I. Klich and L. Levitov, Quantum noise as an entanglement meter, *Phys. Rev. Lett.* **102**, 100502 (2009).
- [31] B. Hsu, E. Grosfeld, and E. Fradkin, Quantum noise and entanglement generated by a local quantum quench, *Phys. Rev. B* **80**, 235412 (2009).
- [32] H. F. Song, S. Rachel, and K. Le Hur, General relation between entanglement and fluctuations in one dimension, *Phys. Rev. B* **82**, 012405 (2010).
- [33] H. F. Song, N. Laflorencie, S. Rachel, and K. Le Hur, Entanglement entropy of the two-dimensional heisenberg antiferromagnet, *Phys. Rev. B* **83**, 224410 (2011).
- [34] H. F. Song, S. Rachel, C. Flindt, I. Klich, N. Laflorencie, and K. Le Hur, Bipartite fluctuations as a probe of many-body entanglement, *Phys. Rev. B* **85**, 035409 (2012).
- [35] P. Calabrese, M. Mintchev, and E. Vicari, Exact relations between particle fluctuations and entanglement in fermi gases, *EPL (Europhysics Letters)* **98**, 20003 (2012).
- [36] S. Rachel, N. Laflorencie, H. F. Song, and K. Le Hur, Detecting quantum critical points using bipartite fluctuations, *Phys. Rev. Lett.* **108**, 116401 (2012).
- [37] R. Süssstrunk and D. A. Ivanov, Free fermions on a line: Asymptotics of the entanglement entropy and entanglement spectrum from full counting statistics, *EPL (Europhysics Letters)* **100**, 60009 (2012).
- [38] B. Swingle, Rényi entropy, mutual information, and fluctuation properties of fermi liquids, *Phys. Rev. B* **86**, 045109 (2012).
- [39] E. Vicari, Entanglement and particle correlations of fermi gases in harmonic traps, *Phys. Rev. A* **85**, 062104 (2012).
- [40] V. Eisler, Universality in the full counting statistics of trapped fermions, *Phys. Rev. Lett.* **111**, 080402 (2013).
- [41] I. Klich, A note on the full counting statistics of paired fermions, *Journal of Statistical Mechanics: Theory and Experiment* **2014**, P11006 (2014).
- [42] A. Petrescu, H. F. Song, S. Rachel, Z. Ristivojevic, C. Flindt, N. Laflorencie, I. Klich, N. Regnault, and K. L. Hur, Fluctuations and entanglement spectrum in quantum hall states, *Journal of Statistical Mechanics: Theory and Experiment* **2014**, P10005 (2014).
- [43] P. Calabrese, M. Mintchev, and E. Vicari, Entanglement entropy of one-dimensional gases, *Phys. Rev. Lett.* **107**, 020601 (2011).
- [44] P. Calabrese, M. Mintchev, and E. Vicari, Entanglement entropies in free-fermion gases for arbitrary dimension, *EPL (Europhysics Letters)* **97**, 20009 (2012).
- [45] C. Varma, P. B. Littlewood, S. Schmitt-Rink, E. Abrahams, and A. Ruckenstein, Phenomenology of the normal state of cu-o high-temperature superconductors, *Physical Review Letters* **63**, 1996 (1989).
- [46] P. B. Littlewood and C. M. Varma, Phenomenology of the superconductive state of a marginal fermi liquid, *Phys. Rev. B* **46**, 405 (1992).
- [47] A. Ruckenstein and C. Varma, A theory of marginal fermi-liquids, *Physica C: Superconductivity* **185-189**, 134 (1991).
- [48] A. Mukherjee and S. Lal, Scaling theory for mott-hubbard transitions: I. $t = 0$ phase diagram of the $1/2$ -filled hubbard model, *New Journal of Physics* **22**, 063007 (2020).
- [49] A. Mukherjee and S. Lal, Scaling theory for mott-hubbard transitions-II: quantum criticality of the doped mott insulator, *New Journal of Physics* **22**, 063008 (2020).
- [50] A. Mukherjee and S. Lal, Holographic unitary renormalization group for correlated electrons - ii: Insights on fermionic criticality, *Nuclear Physics B* **960**, 115163 (2020).
- [51] B. Swingle and T. Senthil, Universal crossovers between entanglement entropy and thermal entropy, *Phys. Rev. B* **87**, 045123 (2013).
- [52] J. M. Luttinger and J. C. Ward, Ground-state energy of a many-fermion system. ii, *Physical Review* **118**, 1417 (1960).
- [53] M. Oshikawa, Topological approach to luttinger's theorem and the fermi surface of a kondo lattice, *Physical Review Letters* **84**, 3370 (2000).
- [54] I. Dzyaloshinskii, Some consequences of the luttinger theorem: The luttinger surfaces in non-fermi liquids and mott insulators, *Physical Review B* **68**, 085113 (2003).
- [55] K. Seki and S. Yunoki, Topological interpretation of the luttinger theorem, *Physical Review B* **96**, 085124 (2017).
- [56] J. T. Heath and K. S. Bedell, Necessary and sufficient conditions for the validity of luttinger's theorem, *New Journal of Physics* **22**, 063011 (2020).
- [57] A. Mukherjee and S. Lal, Holographic unitary renormalization group for correlated electrons - i: A tensor network

- approach, *Nuclear Physics B* **960**, 115170 (2020).
- [58] A. Mukherjee, S. Patra, and S. Lal, Fermionic criticality is shaped by fermi surface topology: a case study of the tomonaga-luttinger liquid, *Journal of High Energy Physics* **2021**, 148 (2021).
- [59] R. Shankar, Renormalization-group approach to interacting fermions, *Reviews of Modern Physics* **66**, 129 (1994).
- [60] J. Polchinski, Effective field theory and the fermi surface, arXiv preprint hep-th/9210046 (1992).
- [61] V. Balasubramanian, M. B. McDermott, and M. Van Raamsdonk, Momentum-space entanglement and renormalization in quantum field theory, *Physical Review D* **86**, 045014 (2012).
- [62] T. Grover and M. P. A. Fisher, Quantum disentangled liquids, *Journal of Statistical Mechanics: Theory and Experiment* **2014**, P10010 (2014).
- [63] T. Grover and M. P. A. Fisher, Entanglement and the sign structure of quantum states, *Phys. Rev. A* **92**, 042308 (2015).
- [64] N. Kaplis, F. Krueger, and J. Zaanen, Entanglement entropies and fermion signs of critical metals, *Physical Review B* **95**, 155102 (2017).
- [65] S. Patra and S. Lal, Origin of topological order in a cooper-pair insulator, *Phys. Rev. B* **104**, 144514 (2021).
- [66] S. Pal, A. Mukherjee, and S. Lal, Correlated spin liquids in the quantum kagome antiferromagnet at finite field: a renormalization group analysis, *New Journal of Physics* **21**, 023019 (2019).
- [67] A. Mukherjee, A. Mukherjee, N. S. Vidhyadhiraja, A. Taphader, and S. Lal, Unveiling the kondo cloud: Unitary renormalization-group study of the kondo model, *Phys. Rev. B* **105**, 085119 (2022).
- [68] A. Mukherjee and S. Lal, Superconductivity from repulsion in the doped 2d electronic hubbard model: an entanglement perspective, *Journal of Physics: Condensed Matter* (2022).
- [69] P. W. Anderson, Random-phase approximation in the theory of superconductivity, *Physical Review* **112**, 1900 (1958).
- [70] C. H. Lee, P. Ye, and X.-L. Qi, Position-momentum duality in the entanglement spectrum of free fermions, *J. Stat. Mech.: Theory and Expt.*, P10023 (2014).
- [71] J. Maldacena, The large-n limit of superconformal field theories and supergravity, *International journal of theoretical physics* **38**, 1113 (1999).
- [72] E. Witten, Anti de sitter space and holography, arXiv preprint hep-th/9802150 (1998).
- [73] X.-L. Qi, Exact holographic mapping and emergent space-time geometry, arXiv preprint arXiv:1309.6282 (2013).
- [74] C. H. Lee and X.-L. Qi, Exact holographic mapping in free fermion systems, *Physical Review B* **93**, 035112 (2016).
- [75] S. Patra, S. Basu, and S. Lal, Unveiling topological order through multipartite entanglement, *Phys. Rev. A* **105**, 052428 (2022).
- [76] S. Ryu and T. Takayanagi, Aspects of holographic entanglement entropy, *Journal of High Energy Physics* **2006**, 045 (2006).
- [77] M. Levin and X.-G. Wen, Detecting topological order in a ground state wave function, *Phys. Rev. Lett.* **96**, 110405 (2006).

SUPPLEMENTARY MATERIALS FOR “UNIVERSAL ENTANGLEMENT SIGNATURES OF QUANTUM LIQUIDS AS A GUIDE TO FERMIONIC CRITICALITY”

I. UNITARY RENORMALIZATION GROUP METHOD

The URG method iteratively decouples quantum fluctuations in higher energy Fock states by applying a many-body unitary operator, generating thereby a low-energy effective Hamiltonian. For a general electronic system with Hamiltonian $\mathcal{H}_{(N)}$ with total N Fock states, Mutually non-commuting terms in the Hamiltonian are the source of quantum fluctuation in the occupation of the electronic Fock states. We first label the Fock states according to the eigenvalues of the diagonal part of the bare Hamiltonian, $\epsilon_N > \epsilon_{N-1} > \dots$. The unitary operator \mathcal{U}_N then decoupled the N^{th} Fock state from all other states, i.e., it removes quantum fluctuation present in this state. The low-energy effective Hamiltonian after the first step of URG is

$$\mathcal{H}_{(N-1)} = \mathcal{U}_N \mathcal{H}_{(N)} \mathcal{U}_N^\dagger. \quad (7)$$

Subsequently, the unitary operator \mathcal{U}_{N-1} is used to remove the quantum fluctuations in the Fock state $N-1$, and so on. The general form of the unitary operator for j^{th} step of URG is given as

$$\begin{aligned} \mathcal{U}_j &= (1 + \eta_j - \eta_j^\dagger)/\sqrt{2}, \\ \eta_j^\dagger &= \frac{1}{\omega - \text{Tr}(\mathcal{H}_{(j)} \hat{n}_j)} c_j^\dagger \text{Tr}(\mathcal{H}_{(j)} c_j), \end{aligned} \quad (8)$$

where ω characterises the energyscale for quantum fluctuations, and an equivalence of ω has been established with that for thermal fluctuations at a finite-temperature [48–50, 57]. Iterative application of the unitaries generates a series of effective Hamiltonians with progressively lower RG energy scale, $\mathcal{H}_{(N)}, \mathcal{H}_{(N-1)}, \dots$. The fixed point effective theory is reached at the effective Hamiltonian $\mathcal{H}_{(j^*)}$, when further decoupling is not possible due to the vanishing of the denominator of η_{j^*} . At any step of the URG [48–50, 57, 58, 65, 66, 68], the Hamiltonian in the rotated basis is given by

$$U_{k\sigma} \hat{H} U_{k\sigma}^\dagger = \frac{1}{2} \text{Tr}_{k\sigma}(\hat{H}) + \tau_{k\sigma} \text{Tr}_{k\sigma}(H \tau_{k\sigma}) + \tau_{k\sigma} \{c_{k\sigma}^\dagger \text{Tr}_{k\sigma}(\hat{H} c_{k\sigma}), \hat{n}_{k\sigma}\}. \quad (9)$$

It is important to note that while $\hat{n}_{k\sigma} \hat{H} (1 - \hat{n}_{k\sigma}) \neq 0$ (i.e., there exist non-trivial quantum fluctuations in the occupation of single-particle Fock state given by n_σ) prior to the application of the unitary operator, the unitary operation removes

such quantum fluctuation.

$$\hat{n}_{k\sigma} U_{k\sigma} \hat{H} U_{k\sigma}^\dagger (1 - \hat{n}_{k\sigma}) = 0 \Rightarrow [\hat{n}_{k\sigma}, U_{k\sigma} \hat{H} U_{k\sigma}^\dagger] = 0, \quad (10)$$

upon the application of U . The degree of freedom $n_{k\sigma}$ is thus rendered an integral of motion (IOM) of the RG flow. The RG equations can then be obtained from the condition eq.(10). The diagonal part of the Hamiltonian $H_{(k\sigma)}^D$ with respect to the Fock state $(k\sigma)$ has the property $[H_{(k\sigma)}^D, \hat{n}_{k\sigma}] = 0$. Then, the operators $\eta_{k\sigma}^\dagger$ and $\eta_{k\sigma}$ are given as

$$\begin{aligned} \eta_{k\sigma}^\dagger &= \frac{1}{\hat{\omega}_{k\sigma} - Tr_N(\hat{n}_{k\sigma} H_{(k\sigma)}^D) \hat{n}_{k\sigma}} Tr_{k\sigma}(H_{(k\sigma)} c_{k\sigma}) c_{k\sigma}^\dagger, \\ \eta_{k\sigma} &= \frac{1}{\hat{\omega}_{k\sigma} - Tr_{k\sigma}((1 - \hat{n}_{k\sigma}) H_{(k\sigma)}^D)(1 - \hat{n}_{k\sigma})} c_{k\sigma} Tr_{k\sigma}(c_{k\sigma}^\dagger H_{(k\sigma)}). \end{aligned} \quad (11)$$

For this work, we obtain the effective Hamiltonian for the FL and MFL by performing a URG analysis of the 2D Hubbard model [48, 49]. The Hamiltonian RG flow equation is

$$\Delta H_{(j)} = \sum_l Tr_{j,l}(c_{j,l}^\dagger) c_{j,l} G_{(j),l} c_{j,l}^\dagger Tr_{j,l}(H_{(j)} c_{j,l}), \quad (12)$$

where $G_{(j),l} = [\omega - \hat{n}_{j,l} Tr_{j,l}(H_{(j)}^D \hat{n}_{j,l})]^{-1}$ and $H_{(j)}^D$ is the diagonal part of the Hamiltonian at the RG step j . This change in the Hamiltonian is then decomposed in different scattering channels: namely, forward scattering $\Delta H_{(j)}^F$, backscattering $\Delta H_{(j)}^B$, tangential scattering $\Delta H_{(j)}^T$, and the 3-particle interaction term $\Delta H_{(j)}^3$. This leads to the following RG equations

$$\Delta H_{(j)}^F = \sum_{k,k',l'} c_{k',l}^\dagger c_{k',l'}^\dagger \frac{4(V(\delta)_l^{(j)})^2 \tau_{j,l} \tau_{j,l'}}{G_{j,l}^{-1} - V(\delta)_l^{(j)} \tau_{j,l} \tau_{j,l'}} c_{k,l'} c_{k,l}, \quad \text{where } \tau_{j,l} = (\hat{n}_{j,l} - \frac{1}{2}) \quad (13)$$

$$\Delta H_{(j)}^B = \sum_{k,k',l'} c_{k',l}^\dagger c_{k',l'}^\dagger \frac{4V(\delta)_l^{(j)} K(\delta)_l^{(j)} \tau_{j,l} \tau_{j,l'}}{G_{j,l}^{-1} - V(\delta)_l^{(j)} \tau_{j,l} \tau_{j,l'}} c_{k,l'} c_{k,l}, \quad (14)$$

$$\Delta H_{(j)}^T = \sum_{k,k',m,n} c_{k,m}^\dagger c_{k,m'}^\dagger \frac{(\Gamma^{(j)})^2 (L_j^2 - L_j^{z2} - L_j^z)}{\omega - \tilde{\epsilon}_{j,avg}^c L_j^z - \Gamma^{(j)} L_j^{z2}} c_{k',n'} c_{k',n}, \quad (15)$$

$$\begin{aligned} \Delta H_{(j)}^3 &= \sum_{k'',k',l',l''} c_{k',l}^\dagger c_{k',l'}^\dagger c_{j,l} \frac{V_l^{(j)}(\delta) V_l^{(j)}(\delta') \tau_{j,l}}{\omega - \tilde{\epsilon}_{j,l} \tau_{j,l}} c_{j,l''}^\dagger c_{k'',l''} c_{k'',l'} + \sum_{k'',p',l',l''} c_{p',l}^\dagger c_{p',l'}^\dagger c_{j,l'} \frac{K_l^{(j)}(\delta) K_l^{(j)}(\delta') \tau_{j,l}}{\omega - \tilde{\epsilon}_{j,l} \tau_{j,l}} c_{j,l''}^\dagger c_{k'',l''} c_{k'',l'} \\ &+ \sum_{\Lambda' < \Lambda_j, p', k''} c_{p',l}^\dagger c_{p',l'}^\dagger c_{j',l'} \frac{8R_{l,\delta\delta''}^{(j)} R_{l,\delta'\delta''}^{(j)} \tau_{i_1} \tau_{i_2} \tau_{i_3}}{G_{j,l,3}^{-1} - R_{l,\delta'',\delta''}^{(j)} \tau_{i_1} \tau_{i_2} \tau_{i_3}} c_{j,l''}^\dagger c_{k'',l''} c_{k'',l'}. \end{aligned} \quad (16)$$

In the above equations, (j, l) represents the state $|\vec{k}_{\Lambda_j, \hat{s}\sigma}\rangle$, $(j, l') \equiv |\vec{k}_{-\Lambda_j + \delta, T\hat{s}\sigma}\rangle$, and $(j', l) \equiv |\vec{k}_{\Lambda_j, \hat{s}\sigma}\rangle$. Further, $V(\delta)_l^{(j)}$, $K(\delta)_l^{(j)}$ and $\Gamma_l^{(j)}$ are the forward scattering density-density interaction, backscattering and tangential scattering couplings respectively, while $R_{\delta\delta}^{(j)}$ is the interaction coupling for the 3-particle (i.e., 2-electron-1-hole) composites objects. δ represents the off-resonant scattering momenta. The components of the pseudospin \vec{L} , $L^+ = \sum_m c_{j,m}^\dagger c_{j,m'}^\dagger$, $L_j^z = (1/2) \sum_m (\hat{n}_{j,m} + \hat{n}_{j,m'} - 1)$ etc. follow the standard spin-algebra. Further, the electronic Fock states are labelled as $i_1 : (\vec{k}_{\Lambda_j, \hat{s}, \sigma})$, $i_2 : (\vec{k}_{-\Lambda_j + \delta'', T\hat{s}, -\sigma})$, $i_3 : (\vec{k}_{\Lambda', \hat{s}, \sigma})$. $G_{j,l,3}^{-1} = (\epsilon_{j,l} + \epsilon_{j,l'})/2 - \Delta\mu_{eff} - \omega$, where ω is the quantum fluctuation scale. From eq.(12), we extract the coupling RG equations as follows

$$\Delta V_{l,\hat{s}}^{(j)} = -\frac{(V_{l,\hat{s}}^{(j)})^2}{\frac{1}{2}E_{j,\hat{s}} - \omega + \frac{1}{4}V_{l,\hat{s}}^{(j)}}, \quad (17)$$

$$\Delta K_{l,\hat{s}}^{(j)} = -\frac{(K_{l,\hat{s}}^{(j)})^2}{\omega - \frac{1}{2}E_{j,\hat{s}} + \frac{1}{4}K_{l,\hat{s}}^{(j)}}, \quad (18)$$

$$\Delta \Gamma_{\hat{s}}^{(j)} = -\frac{N_F^2 (\Gamma_{\hat{s}}^{(j)})^2}{\frac{1}{N_F} \sum_s E_{j,\hat{s}} - \omega + \frac{1}{4}\Gamma_{\hat{s}}^{(j)}}, \quad (19)$$

$$\Delta R_{l,\hat{s}}^{(j)} = \frac{(V_{l,\hat{s}}^{(j)})^2}{\omega - \epsilon_{j,\hat{s}}} + \frac{(K_{l,\hat{s}}^{(j)})^2}{\omega - \epsilon_{j,\hat{s}}} + \frac{(R_{l,\hat{s}}^{(j)})^2}{\frac{1}{2}E_{j,\hat{s}} - \omega + \frac{1}{8}R_{l,\hat{s}}}, \quad (20)$$

where $E_{j,\hat{s}} = (\epsilon_{\Lambda_j, \hat{s}} + \epsilon_{\Lambda_j, -\hat{s}} - 2\Delta\mu_{eff})$, and $\Delta\mu_{eff} = -\Delta U/2$, N_F is the number of electronic states on the Fermi surface, and $\epsilon_{\Lambda_j, \hat{s}}$ is the kinetic energy of an electron lying on the direction \hat{s} normal to the Fermi surface and at a momentum-space distance Λ_j

from the Fermi energy. It was shown in Refs.[48, 49] that the gapless FL is obtained in the overdoped 2D Hubbard model with the couplings V and Γ dominant under RG, while the MFL is obtained for filling ranging from $1/2$ to optimal hole-doping at sufficiently high quantum fluctuation scale ω due to the coupling R being dominant under the RG flow. Having set out the URG flow to the IR fixed point Hamiltonian, we can now sketch the MERG algorithm. First, we solve for the wavefunctions of the ground state and low-lying excited states of the fixed point Hamiltonian. Now, by acting with the unitary operators of the URG in reverse on, say, the ground state $|\Psi_0\rangle$, we systematically re-entangle the low-energy degrees of freedom lying proximate to the Fermi surface with the hitherto decoupled Fock states (i.e., describing the IOMs of the URG flow). In this way, we generate under the MERG flow a family of many-body wavefunctions that are unitarily connected to $|\Psi_0\rangle$ by quantum fluctuations in momentum-space [58, 65, 67, 68]. The explicit form of the wavefunction obtained after the first step of the MERG flow is given by

$$\begin{aligned} |\Psi_1\rangle &= \frac{1}{\sqrt{2}} \left[1 + Q_{k\sigma} c_{k\sigma} \text{Tr}_{k\sigma} (c_{k\sigma}^\dagger H_{(k\sigma)}) - P_{k\sigma} \text{Tr}_{k\sigma} (H_{(k\sigma)} c_{k\sigma}) c_{k\sigma}^\dagger \right] |\Psi_0\rangle, \\ \hat{Q}_{k\sigma} &= \frac{1}{\hat{\omega}_{k\sigma} - \text{Tr}_{k\sigma} ((1 - \hat{n}_{k\sigma}) H_{(k\sigma)}^D) (1 - \hat{n}_{k\sigma})}, \\ \hat{P}_{k\sigma} &= \frac{1}{\hat{\omega}_{k\sigma} - \text{Tr}_{k\sigma} (\hat{n}_{k\sigma} H_{(k\sigma)}^D) \hat{n}_{k\sigma}}. \end{aligned} \quad (21)$$

Having obtained a series of many-body wavefunctions from the MERG, we compute from them the RG evolution of several measures of many-particle entanglement and many-body correlations.

II. RG EVOLUTION OF VARIOUS MEASURES OF ENTANGLEMENT

A. Many-particle Block Entanglement Entropy (MBE)

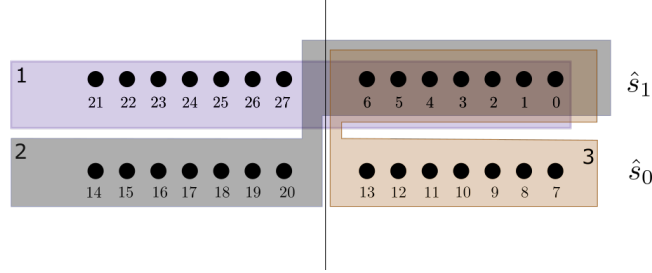


FIG. 7. Three choices of momentum-space blocks to compute block entanglement entropy from each member of the family of wavefunctions obtained from the MERG. *Block-1* includes all the nodes on the direction \hat{s}_1 . *Block-2* includes the nodes outside the Fermi surface on \hat{s}_1 and inside the Fermi surface on \hat{s}_0 . *Block-3* includes all the nodes residing outside the Fermi surface.

As discussed in the main manuscript, we study a prototypical system involving 28 pseudospin degrees of freedom formed from 56 electronic Fock states. While there is no entanglement among the low-energy states that comprise the IR fixed point theory in momentum (or, k)-space, nontrivial entanglement is emergent from the MERG method. This is due to the introduction of RG-irrelevant quantum fluctuations that iteratively couple the low-energy states within the low-energy window (namely, the states 6, 13, 20 and 27) with the 24 states that lie outside it and farther away from the Fermi surface as the MERG flow proceeds towards the UV. We measure the variation of the entanglement entropy of subsystems of blocks of states in k -space in the many-body state with the MERG steps.

As shown in the Fig.7, we have chosen three blocks of states in k -space blocks comprising a total of 14 states. Subsystem choice 1 consists of states along the near-anti-nodal direction \hat{s}_1 normal to the Fermi surface. Thus, the entanglement entropy measured here involves the entanglement between the states in \hat{s}_1 and those in \hat{s}_0 (i.e., the nodal direction normal to the Fermi surface), thus offering a measure of the entanglement driven by quantum fluctuations generated via tangential scatterings between the two \hat{s} directions. Subsystem choice 2, on the other hand, consists of states outside the Fermi surface in \hat{s}_1 but in \hat{s}_0 ; the entanglement entropy measures here the entanglement arising from quantum fluctuations involving both tangential and forward scatterings. Another subsystem choice is that shown in block 3, involving states outside the Fermi surface in both the \hat{s} directions. The entanglement entropy here measures the k -space entanglement driven due to excitations that lead from within states the Fermi surface to those outside it, arising from quantum fluctuations involving both forward and tangential scattering events.

The results presented in Figs.8, 9 and 10) of the variation of the many-particle block entanglement (MBE) with the number of MERG steps show distinctions between the FL and MFL states. As block 1 is very sensitive to entanglement arising from quantum fluctuations due to tangential scattering events, the stark difference between the numbers achieved by the MBE in the UV for the case of block 1 in the FL and MFL reveals the dominance of tangential scattering events in the former over the latter. On the other hand, the similar values of the MBE achieved in the UV for the blocks 2 and 3 shows the importance of forward scattering events in both the FL and MFL phases. Taken together, these results show that while the IR ground state of the FL is obtained from the decoupling of quantum fluctuations that arise from both forward and tangential scattering, the MFL is obtained from the decoupling of quantum fluctuations that arise almost completely from forward scattering.

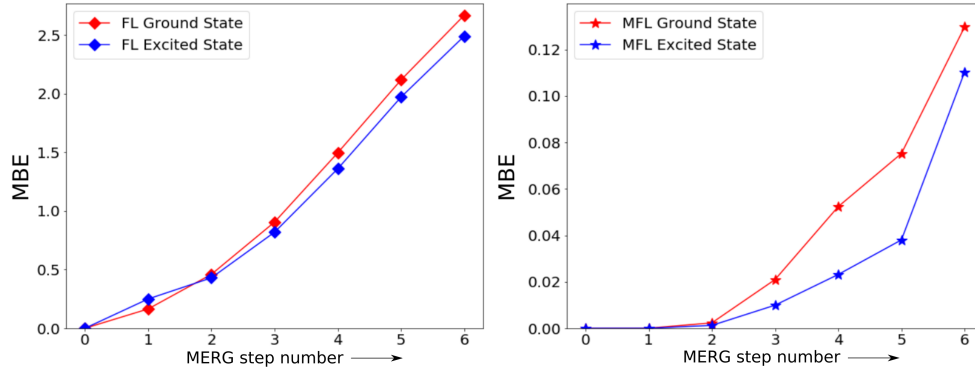


FIG. 8. Variation of the block entanglement entropy for the choice of Block 1 of Fig.7 with MERG step number for FL and MFL ground and nodal excited states. *Left:* Red curve represents the entanglement scaling for the FL ground state, and the blue one represents the FL nodal excited state. *Right:* Red curve represents the entanglement scaling for the MFL ground state, and the blue curve represents MFL nodal excited state.

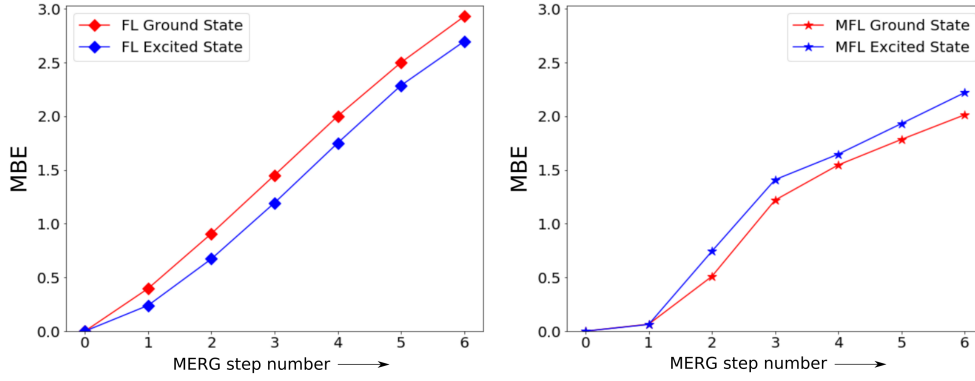


FIG. 9. Variation of the block entanglement entropy for the choice of Block 2 of Fig.7 with MERG step number for FL and MFL ground and nodal excited states. *Left:* Red curve represents the entanglement scaling for the FL ground state, and the blue one represents the FL nodal excited state. *Right:* Red curve represents the entanglement scaling for the MFL ground state, and the blue curve represents MFL nodal excited state.

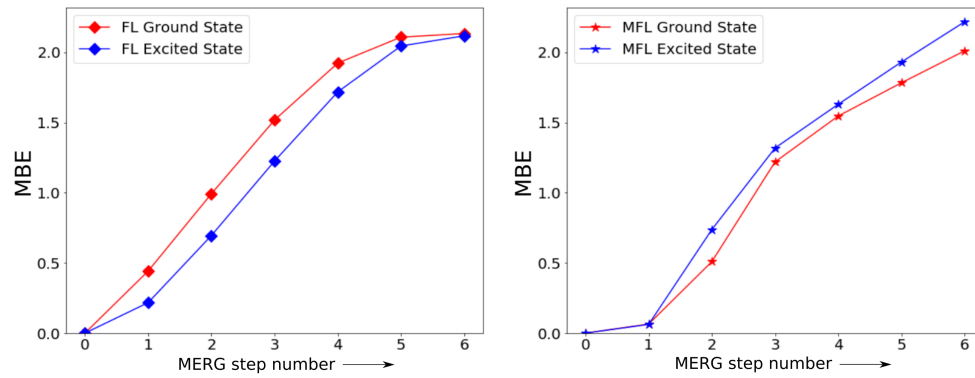


FIG. 10. Variation of the block entanglement entropy for the choice of Block 3 of Fig.7 with the MERG step number for FL and MFL ground and nodal excited states. *Left:* Red curve represents the entanglement scaling for the FL ground state, and the blue one represents the FL nodal excited state. *Right:* Red curve represents the entanglement scaling for the MFL ground state, and the blue curve represents MFL nodal excited state.

B. Ryu-Takayanagi upper bound for Entanglement

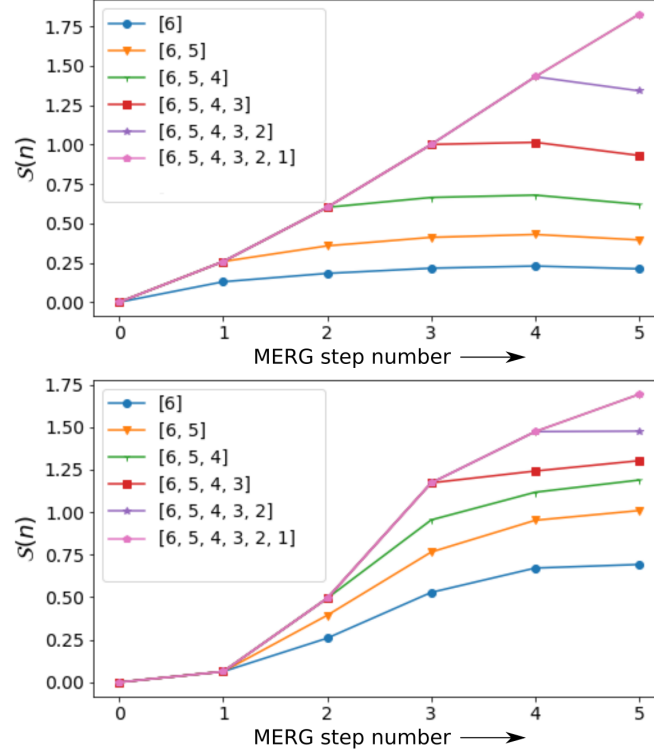


FIG. 11. *Top*: Variation of entanglement entropy of blocks of momentum-space states of varying sizes with MERG step number for the FL ground state. Different coloured curves correspond to different block sizes (shown in inset). *Bottom*: Scaling of entanglement entropy of blocks of momentum-space states of varying sizes with respect to MERG step number with MERG step number for the MFL ground state.

Given that the URG method (from which the unitaries are obtained for the MERG) is known to correspond to an exact holographic mapping [57, 73], we will now check whether the entanglement entropies of various sizes of subsystems taken from the family of many-body wavefunctions generated by the MERG satisfy the Ryu-Takayanagi upper bound [76]. This bound is defined as follows:

$$S_n^{max} \leq n S_1^{max}, \quad (22)$$

where S_n^{max} corresponds to the largest entanglement entropy of a subsystem containing n constituents (and $n \geq 1, n \in \mathcal{Z}$). For this, we first compute the entanglement entropy of various block sizes across the MERG energy scales ranging from the UV to the IR fixed point, as shown in the Figure.11. The blocks have been chosen to lie along the near-anti-nodal direction \hat{s}_1 and outside the Fermi surface. The smallest block size contains one pseudospin state (6), while the largest contains all 7 states residing on the \hat{s}_1 direction outside the Fermi surface (see legends in inset). Fig.11 shows that the block entanglement entropies increase from the IR and increase linearly in the UV for the FL (i.e., for the largest block size (6, 5, 4, 3, 2, 1, 0)), while they saturate for the MFL. This increase in entanglement in the FL phase is likely due to the strong growth of tangential scattering in addition to forward scattering. Fig.12 shows a comparison of $S(6)^{max}$ (associated with the largest block size (6, 5, 4, 3, 2, 1)) for both the FL and MFL with $6 \times S(1)^{max}$, and reveals that the Ryu-Takayanagi upper bound is indeed obeyed for both these gapless quantum liquids. The growth of the upper bound in the UV energy scale for the FL phase (as compared to the saturation witnessed for the MFL phase) is again likely due to the presence of strong tangential scattering processes.

C. Mutual Information

Mutual information between two subsystems measures the total classical as well as quantum correlations between them. Definition of mutual information between two subsystems A and B is given as

$$I_2(A : B) = S(A) + S(B) - S(AB) \geq 0, \quad (23)$$

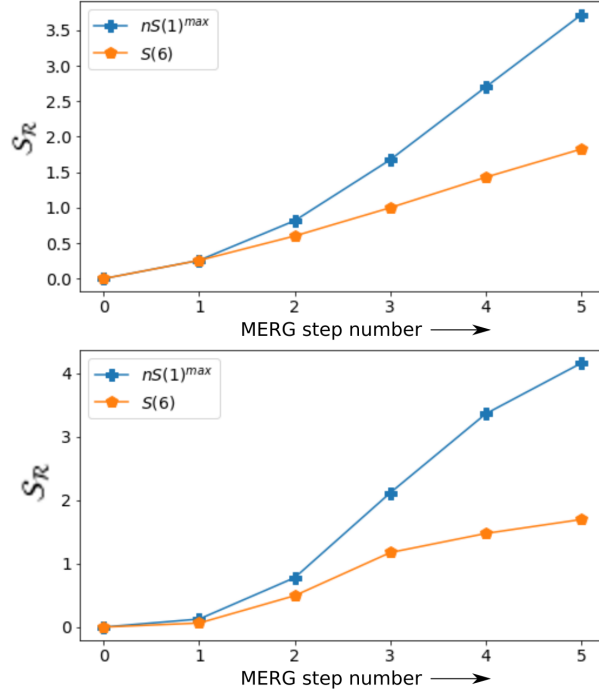


FIG. 12. MERG evolution of the Ryu-Takayanagi upper bound. The blue plus symbols represent the entanglement entropy of the largest block of block size six, and the red pentagons represent the upper bound by $nS(1)^{max}$, where $n = 6$. The *top* and *bottom* figures show that the scaling of the largest block entanglement entropy is satisfied for the FL and MFL phase respectively.

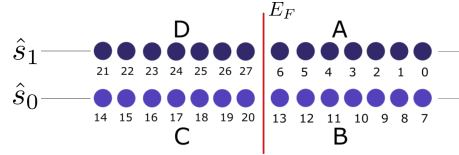


FIG. 13. Prototypical k -space system of 28 pseudospins is divided into four blocks A, B, C and D . The blocks A and B reside outside the Fermi surface, while the blocks C and D reside inside the Fermi surface. E_F represents the Fermi energy. \hat{s}_0 and \hat{s}_1 represents the nodal and near-anti-nodal directions perpendicular to the Fermi surface.

where $S(A_i)$ is the von-Neumann entanglement entropy of the subset A_i with the rest etc. Here, we compute the mutual information between two momentum-space blocks. For this, we divide the entire 28 pseudospin system into four blocks (A, B, C, D), as shown in Fig.13, and compute the mutual information between some of them for each member of the family of wavefunctions generated by the MERG. The scaling of some of these mutual informations is presented in Fig.14. We are mainly interested in the mutual informations $I_2(A, B)$ and $I_2(A, D)$: which capture the correlation arising from tangential and forward scattering. Note that $I_2(A, B)$ captures the correlations between the blocks A and B connected via tangential and forward scattering, whereas $I_2(A, D)$ captures that between A and D connected only through forward scattering. Fig.14(left) shows that $I_2(A, B)$ for the ground and excited states of the FL increases with the number of MERG steps, in keeping with the steady growth in tangential scattering events as the MERG proceeds towards the UV. This is in contrast with our finding for ground and excited states of the MFL case, which remain zero throughout the MERG; this is consistent with RG irrelevant tangential scattering processes for the MFL. Further, the $I_2(A, D)$ among the blocks A, D shown in Fig.14(right) shows the importance of forward scattering is far greater in the UV for the MFL than it is for the FL.

D. Tripartite Information

Tripartite information measures the joint entropy among three subsystems (A, B, C) [5, 75, 77], and is defined as

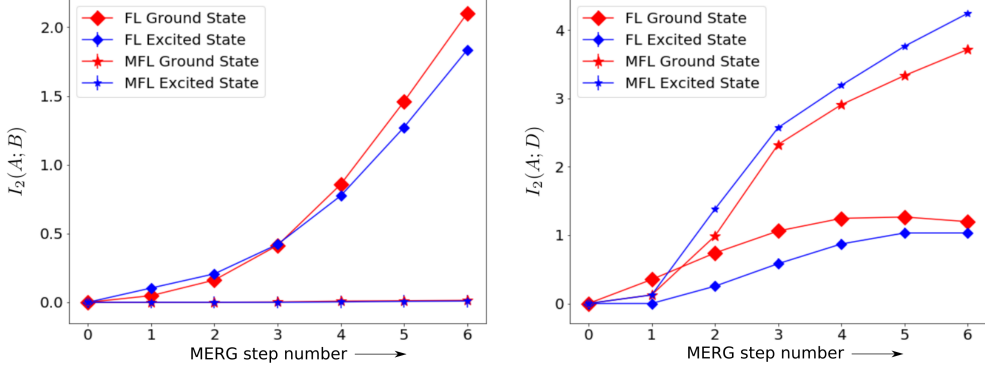


FIG. 14. Variation of Mutual information ($I_2(A; B)$) between blocks A and B (left figure). and Mutual Information ($I_2(A; D)$) between blocks A and D (right figure) with MERG step number.

$$\begin{aligned} I_3(A, B, C) &= S(A) + S(B) + S(C) - S(A \cup B) - S(B \cup C) - S(C \cup A) + S(A \cup B \cup C) , \\ &= I_2(A, B) + S(C) - S(B \cup C) - S(C \cup A) + S(A \cup B \cup C) . \end{aligned} \quad (24)$$

We are mainly interested in the tripartite information among the three pseudospin states (20, 27, 6) proximate to the Fermi surface:

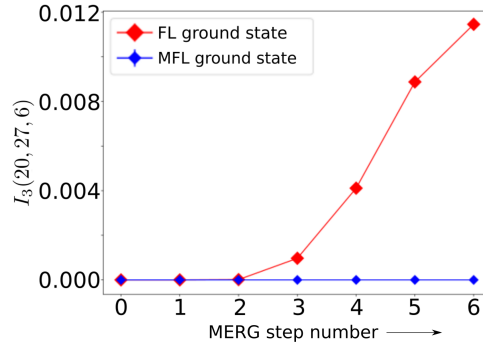


FIG. 15. Variation of the tripartite information $I_3(20, 27, 6)$ among the pseudospin states (20, 27, 6) with MERG step number for the FL (large red diamond) and MFL (small blue diamond) ground states.

the states 6, 27 and 20, 27 are connected via forward and tangential scattering respectively. The MERG scaling of $I_3(6, 20, 27)$ for the FL and MFL ground states is shown in Figure.15: while $I_3(6, 20, 27)$ is found to grow monotonically for the FL as the MERG proceeds to the UV, it is found to remain strictly zero throughout for the MFL. As seen above for the mutual informations, the growth of $I_3(6, 20, 27)$ for the FL is clearly driven by the growth in tangential scattering processes in the UV. Interestingly, the strict vanishing of $I_3(6, 20, 27)$ for the MFL ground state appears to show a constraint among various entanglement measures

$$I_3(6, 20, 27) = S(6) - S(20, 6) - S(27, 6) + S(20, 27, 6) = 0 , \quad (25)$$

where we have used the fact that $I_2(20, 27) = 0$ in the MFL ground state. We note, however, that the individual von-Neumann entanglement entropies in eq.(25) are nonzero. Thus, the relations $I_2(20, 27) = 0$ and $I_3(6, 20, 27) = 0$ appear to be invariants of the MERG flow, capturing the decoupling between various \hat{s} directions normal to the Fermi surface for the MFL.

III. RG EVOLUTION OF VARIOUS MANY-BODY CORRELATIONS

A. Correlations generated due to pseudospin-flip scattering

The low-energy window is formed by the states (6, 13, 2, 27) proximate to the Fermi surface at the IR fixed point, and increases as the MERG progresses towards the UV. We define a correlation measure $C_{sf}^{(j), \hat{s}_1}$ in order to capture the pseudospin-flip correlations among the pseudospin states present in the low-energy window near the near-anti-nodal direction \hat{s}_1

$$C_{sf}^{(j), \hat{s}_1} = \left(\langle \Psi^{(j)} | \sum_{i < j}^{U_{em}^{\hat{s}_1}} (S_i^+ S_j^- + S_j^- S_i^+) | \Psi^{(j)} \rangle \right) / \left(\sum_{i < j}^{U_{em}^{\hat{s}_1}} 1 \right) , \quad (26)$$

where $|\Psi^{(j)}\rangle$ is the wave function at the j^{th} MERG step (i.e., $j = 0$ represents the IR fixed point and increases towards the UV), \mathcal{U}_{em} is the set of pseudospin states lying in the direction \hat{s}_1 within the low-energy window at the j^{th} MERG step. (Note that \mathcal{U}_{em} does not include the decoupled electronic Fock states present outside the emergent window.) As shown in Fig.16(left), the MERG

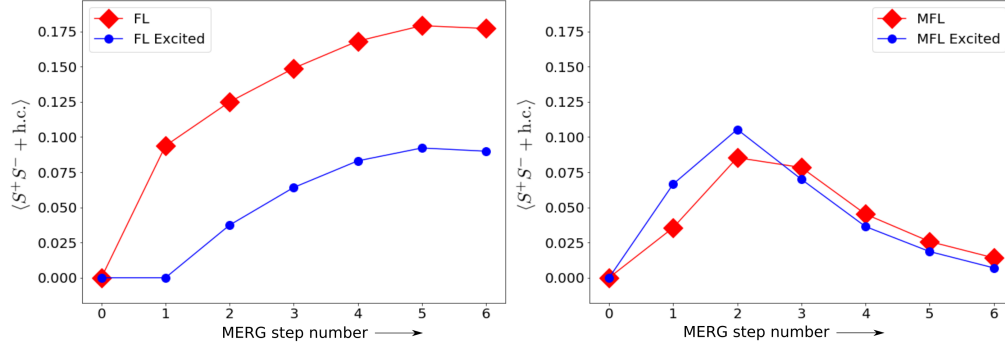


FIG. 16. Variation of the correlations generated by pseudospin-flip scattering processes ($\langle S^+ S^- + \text{h.c.} \rangle$) within the low-energy window with MERG step number. *Left:* Red and blue curves show variation of the correlation for the FL ground and excited state respectively. *Right:* Red and blue curves show variation of the correlation scaling for the MFL ground and excited states respectively.

scaling of the correlation $C_{sf}^{(j),\hat{s}_1}$ for the FL ground and excited states increases and finally saturates in the UV scale. This is due to the fact that the phase space for tangential scattering grows monotonically with the MERG. On the other hand, $C_{sf}^{(j),\hat{s}_1}$ correlation shows a non-monotonic behaviour for the MFL case (Fig.16(right)), likely arising due to an initial increase in the phase space for forward scattering at the beginning of the MERG flow and its eventual decrease as the flow reaches the UV (and highlights the absence of tangential scattering in the MFL).

B. MERG scaling of the occupation of pseudospin states

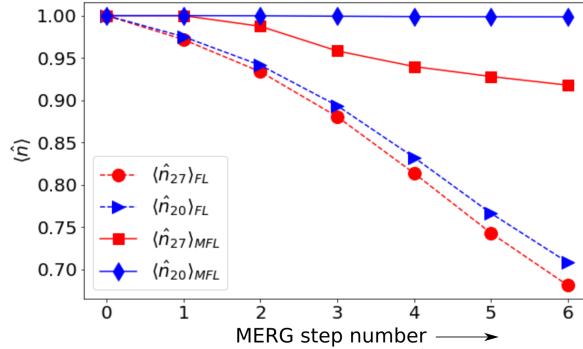


FIG. 17. Variation of the expectation value of the occupation of the states 20 and 27 with MERG step number for the FL and MFL ground states.

Fig.17 shows the MERG flow of the average number occupation of the pseudospin states 20 and 27 (just below the Fermi surface) for both the FL and MFL ground states shown. We see that both $\langle \hat{n}_{20} \rangle$ (blue triangle) and $\langle \hat{n}_{27} \rangle$ decay much faster for the FL (curves with blue triangles and red circles respectively) than for the MFL (curves with blue diamonds and red squares respectively). The similar nature of decays for the FL shows the weak electronic differentiation between the directions \hat{s}_0 and \hat{s}_1 due to the strong tangential scattering. On the other hand, $\langle \hat{n}_{20} \rangle$ does not decay at all under the MERG flow for the MFL ground state while $\langle \hat{n}_{27} \rangle$ decays slowly, displaying the electronic differentiation inherent in the MFL.

C. Non-local strings

Another way by which to probe how tangential and forward scattering shape the FL and MFL states can be learnt by computing the MERG evolution of the expectation value of the k -space non-local operator $Z = \prod_k \sigma_k^z$, $\langle Z \rangle$ for appropriately chosen strings of pseudospin states in k -space. As shown in Fig.18, we have chosen two strings of length 14 nodes each for our analysis. The string

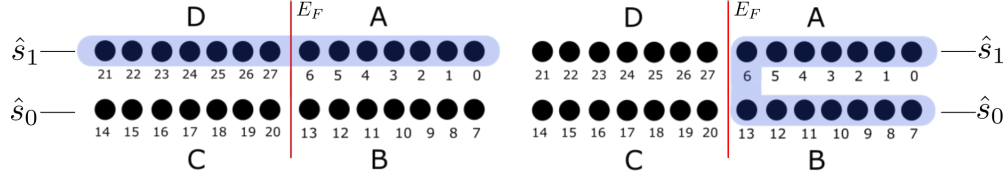


FIG. 18. Two choices of the non-local string parity operators. *Left*: String AD containing states in only one direction perpendicular to the Fermi surface (\hat{s}_1), and stretching across the Fermi surface. *Right*: String AB lying outside the Fermi surface but spread over both \hat{s} directions \hat{s}_0 and \hat{s}_1 .

AD passes across the Fermi surface but along only the near-anti-nodal direction \hat{s}_1 , whereas the string AB lies completely outside the Fermi surface but across the two \hat{s} directions. The operator Z corresponds to a parity operator defined for the pseudospin states in k -space, i.e., sign of $\langle Z \rangle$ depends on the number of down pseudospins: negative for an odd number of down pseudospins (odd parity) and positive for an even number of down pseudospins (even parity). First, we find from Fig.19(left) that $\langle Z_{AD} \rangle$ undergoes a

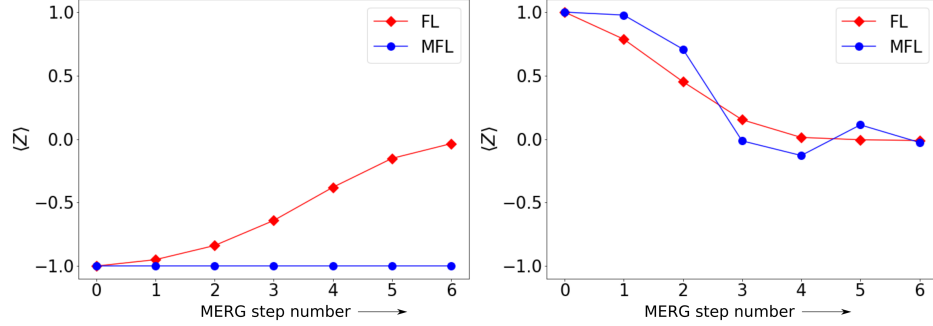


FIG. 19. Variation of the expectation value of the non-local string operator $\langle \hat{Z} \rangle$ for two different string choices AD (left plot) and AB (right plot) (shown in Fig.18) with MERG step number. The blue curve shows variation for the MFL ground state, and the red curve for the FL ground state.

crossover for the FL ground state under the MERG flow from a state with a well-defined parity in the IR ($\langle Z_{AD} \rangle = -1$) to one that does not have a well-defined parity ($\langle Z_{AD} \rangle = 0$) in the UV likely due to the increased tangential scattering. On the other hand, $\langle Z_{AD} \rangle = -1$ for the MFL throughout the MERG flow, i.e., the MFL ground state maintains its parity under forward scattering. Secondly, $\langle Z_{AB} \rangle$ undergoes a crossover under the MERG flow for both the FL and the MFL from states with a well-defined parity ($\langle Z_{AB} \rangle = +1$) to one that does not have a well-defined parity ($\langle Z_{AB} \rangle = 0$). In the MFL, this arises from the absence of tangential scattering between subsystems A and B . On the other hand, the vanishing of $\langle Z_{AB} \rangle$ for the FL likely arise from the tangential scattering events that connect states inside the Fermi surface to those outside (D with B , and C with A).

D. Fidelity in RG scale

Fidelity is a measure of overlap between two wavefunctions defined as $F(\alpha, \beta) = |\langle \psi_\alpha | \psi_\beta \rangle|^2$. We now study the fidelity between the wavefunctions of the FL and MFL ground and excited states as the MERG proceeds from IR to UV. We define $|\Psi_{G/E,0}^{FL}\rangle$ and $|\Psi_{G/E,0}^{MFL}\rangle$ as the IR fixed-point ground (G) and excited (E) state wavefunctions for the FL and MFL phases respectively. Similarly, $|\Psi_{G/E,i}^{FL}\rangle, |\Psi_{G/E,i}^{MFL}\rangle$ are the ground (G) and excited (E) state wavefunctions for the FL and MFL at the i^{th} MERG step. Then, we define the four possible fidelities between the ground and excited state wavefunctions of the FL and MFL phases at the 0^{th} and i^{th} MERG steps as given by $F(\alpha\beta, i) = \langle \Psi_{\alpha,0}^{FL} | \Psi_{\beta,i}^{MFL} \rangle$, where the indices α and β can either be G (ground state) or E (excited state). The MERG flow of the four different fidelities $F(\alpha\beta, i) = \langle \Psi_{\alpha,0}^{FL} | \Psi_{\beta,i}^{MFL} \rangle$ is shown in Fig.20.

We can see from Fig.20(left) that the fidelity between the FL and MFL ground states is perfect at the IR fixed point, $F_{GG,i=0} = 1$. This is simply because both these gapless quantum liquids satisfy Luttinger's theorem, and have the same ground state. However, F_{GG} falls monotonically to zero. On the other hand, the IR excited states of the FL and MFL are orthogonal to the common IR ground state and to one another, as indicated by the near vanishing of the other three fidelities at the zeroth MERG step. Further, this orthogonality is maintained under the MERG flow to the UV, as the unitary operations of the MERG maintain the orthogonality structure of these states. Fig.20(right) shows that the MERG evolution of the square of the real part of the fidelities $F(\alpha\beta, i)$ follows the same trend as $F(\alpha\beta, i)$ itself, reinforcing the fact that the phases of the four fidelities do not play an important role.

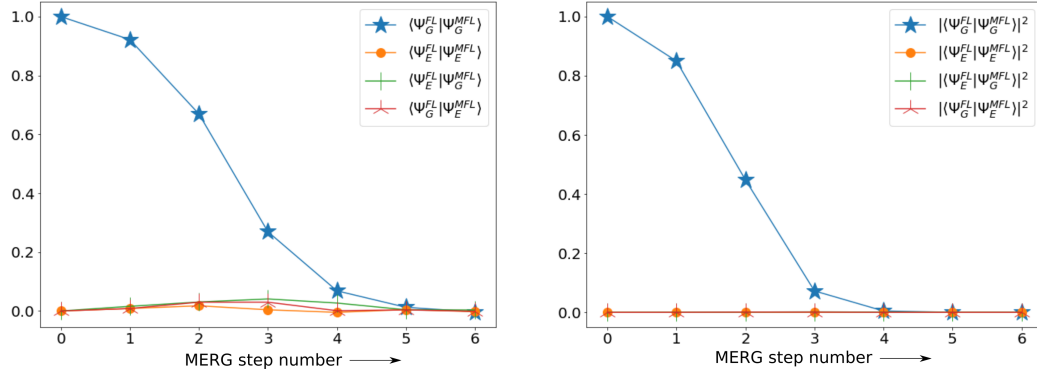


FIG. 20. *Left:* Variation of four fidelities $F(\alpha\beta, i) = \langle \Psi_{\alpha,0}^{FL} | \Psi_{\beta,i}^{MFL} \rangle$, constructed using the overlaps of the FL and MFL ground and excited states (i.e., the indices α and β can either be G (ground state) or E (excited state)), with MERG step number. *Right:* This shows the square of the absolute value of the four fidelities $F(\alpha\beta, i) = \langle \Psi_{\alpha,0}^{FL} | \Psi_{\beta,i}^{MFL} \rangle$.